





Planar thermal Hall effects in the Kitaev spin liquid candidate $\text{Na}_2\text{Co}_2\text{TeO}_6$ Hikaru Takeda ¹, Jiancong Mai,¹ Masatoshi Akazawa,¹ Kyo Tamura,¹ Jian Yan ¹, Kalimuthu Moovendaran,² Kalaivanan Raju,² Raman Sankar,² Kwang-Yong Choi ³, and Minoru Yamashita ^{1,*}¹The Institute for Solid State Physics, University of Tokyo, Kashiwa, 277–8581, Japan²Institute of Physics, Academia Sinica, Taipei 11529, Taiwan³Department of Physics, Sungkyunkwan University, Suwon 16419, Republic of Korea

(Received 17 March 2022; revised 19 October 2022; accepted 24 October 2022; published 23 November 2022)

We investigate both the longitudinal thermal conductivity (κ_{xx}) and the planar thermal Hall conductivity (κ_{xy}) in the Kitaev spin liquid candidate of the cobalt-based honeycomb antiferromagnet $\text{Na}_2\text{Co}_2\text{TeO}_6$ in a magnetic field (B) applied along the a - and a^* -axes. A finite κ_{xy} is resolved for both field directions in the antiferromagnetic (AFM) phase below the Néel temperature of 27 K. The temperature dependence of κ_{xy}/T shows the emergence of topological bosonic excitations. In addition, the field dependence of κ_{xy} shows sign reversals at the critical fields in the AFM phase, suggesting the changes in the Chern number distribution of the topological magnons. Remarkably, a finite κ_{xy} is observed in $B \parallel a^*$ between the first-order transition field in the AFM phase and the saturation field, which is prohibited in a disordered state by the two-fold rotation symmetry around the a^* axis of the honeycomb lattice, showing the presence of a magnetically ordered state that breaks the two-fold rotation symmetry. Our results demonstrate the presence of topological magnons in this compound in the whole field range below the saturation field.

DOI: [10.1103/PhysRevResearch.4.L042035](https://doi.org/10.1103/PhysRevResearch.4.L042035)

Topology in condensed matter physics is a powerful concept allowing one to characterize material properties solely by the topological classification without details of materials. For conduction electrons in a metal, the anomalous quantum Hall effect [1] is one of the most celebrated examples of such topological phenomena, in which the topological invariant (called the Chern number) of conduction electrons is responsible for the dissipationless quantized Hall current even in the zero field [2]. In an insulator, topological effects on the heat carriers give rise to thermal Hall effects (THEs), as described by [3,4]

$$\frac{\kappa_{xy}}{T} = \frac{k_B^2}{\hbar} \int \Omega(E) f(E) dE, \quad (1)$$

where $\Omega(E)$ is the energy distribution of the Berry curvature and $f(E)$ is given by the distribution function of the elementary excitations at energy E , demonstrating that one can reveal the topological property of the charge-neutral excitations by the thermal Hall measurements.

For fermions, the Fermi distribution leads to quantized transport dictated by the sum of the Chern numbers of the occupied bands below the Fermi energy. For example, in the quantum spin liquid (QSL) given by the Kitaev Hamiltonian, the nontrivial topology of the Majorana fermions gives rise to the half quantization of the thermal Hall conductivity (κ_{xy})

[5]. In fact, the half-quantized κ_{xy}/T in the Kitaev QSL, which is suggested to be realized in ruthenium or iridium compounds [6], has been reported in $\alpha\text{-RuCl}_3$ by several groups [7–10]. For bosons, on the other hand, their topological transport vanishes in the zero-temperature limit, because the temperature dependence is governed by the Bose distribution function [11]. Such topological THEs of bosons are proposed for topological magnons [12–15], triplons [16], and skyrmions [17,18]. Indeed, the topological THE of magnons was reported recently in a lattice of magnetic skyrmions [19].

Recently, new Kitaev QSL candidates have been put forward for $3d$ compounds [20–22]. The cobalt-based honeycomb antiferromagnet $\text{Na}_2\text{Co}_2\text{TeO}_6$ [23] constitutes a prominent candidate, in which the high-spin d^7 state of Co^{2+} ions forms two-dimensional honeycomb layers of $J_{\text{eff}} = 1/2$ Kramers doublets with a sizable Kitaev interaction term estimated from the neutron scattering experiments [24–27]. At zero field, a zigzag [28–30] or triple-q [31,32] antiferromagnetic (AFM) order occurs below the Néel temperature $T_N = 27$ K. Magnetization measurements under in-plane magnetic fields [25,30,33] show multiple phase transitions at three critical fields in the AFM phase, as well as a possible emergence of a quantum disordered state between the AFM phase and the spin polarized phase above the saturation field ($B_{\text{sat}} \sim 13$ T). The longitudinal thermal conductivity measurements performed under in-plane fields [33] and the thermal Hall conductivity measurements under $B \parallel c$ [34,35] bear a close resemblance to those of $\alpha\text{-RuCl}_3$, implying a possible realization of the Kitaev QSL in $\text{Na}_2\text{Co}_2\text{TeO}_6$ under an in-plane field above ~ 10 T. However, the half-quantized κ_{xy}/T under the in-plane field, the key signature of the Kitaev QSL, has been missing.

*my@issp.u-tokyo.ac.jp

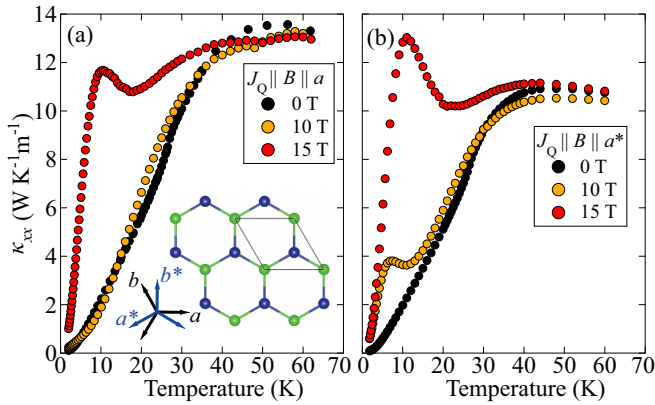


FIG. 1. The temperature dependence of the longitudinal thermal conductivity (κ_{xx}) under various magnetic fields applied along the a - (a) and a^* - (b) axes obtained in the VTI measurements. The inset in (a) illustrates the honeycomb lattice of Co^{2+} ions with the crystallographic axes.

In this Letter, we address the planar THE of $\text{Na}_2\text{Co}_2\text{TeO}_6$ under in-plane magnetic fields. Our salient findings are (i) a finite planar κ_{xy} for both $B \parallel a$ and $B \parallel a^*$, showing the emergence of topological charge-neutral excitations in $\text{Na}_2\text{Co}_2\text{TeO}_6$; (ii) the vanishing temperature dependence of κ_{xy}/T in the zero-temperature limit, consistent with topological bosonic excitations rather than Majorana fermions; and (iii) multiple sign changes of κ_{xy} at critical fields in $B \parallel a$, suggesting changes of the Berry curvature of the topological magnons in different magnetic states.

Single crystals of $\text{Na}_2\text{Co}_2\text{TeO}_6$ were synthesized by the self-flux method as described in Ref. [32]. Prior to the thermal transport measurements, we confirmed the crystallographic directions by x-ray diffraction measurements. Thermal transport measurements were performed by the steady method as described in Ref. [36] by using a variable temperature insert (VTI) for 2 to 60 K and a dilution refrigerator (DR) for 0.1 to 3 K. The heat current J_Q and the magnetic field B were applied parallel to either the a - and a^* -axes of the sample (see Supplemental Material Fig. S1 [37] for more details). The magnetic susceptibility measurements were performed by using a SQUID magnetometer to check the quality and the crystallographic directions of the sample. The reproducibility was confirmed by repeating the κ_{xy} measurements in different single crystals (see Supplemental Material Figs. S4 and S5 [37]).

Figure 1 shows the temperature dependence of the longitudinal thermal conductivity (κ_{xx}) measured under $B \parallel J_Q \parallel a$ [zigzag direction, perpendicular to the honeycomb bond; Fig. 1(a)] and $B \parallel J_Q \parallel a^*$ [“armchair” direction, parallel to the honeycomb bond; Fig. 1(b)]. At zero field, the temperature dependence of κ_{xx} shows a broad peak around 50 K, which is followed by a kink at T_N , as clearly seen in the temperature dependence of κ_{xx}/T (see Supplemental Material Fig. S2 [37]). The Néel transition of the sample is also clearly seen as the peak in the temperature dependence of the magnetic susceptibility (see Supplemental Material Fig. S3 [37]). The good quality of the sample is also confirmed by the boundary-limited phonons observed in κ_{xx} at 15 T (see Supplemental

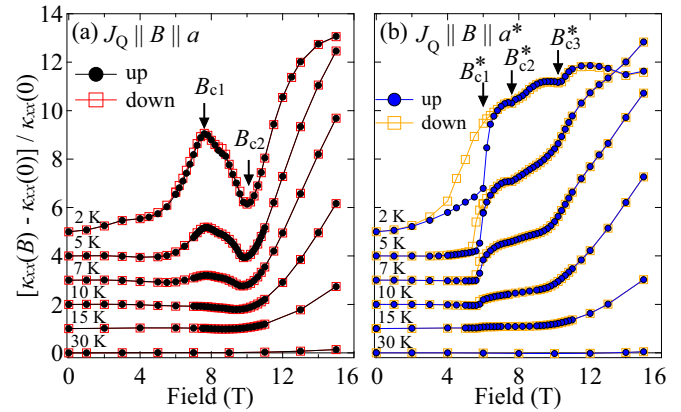


FIG. 2. The field-induced deviation of the longitudinal thermal conductivity $[\kappa_{xx}(B) - \kappa_{xx}(0)] / \kappa_{xx}(0)$ under magnetic fields applied along the a - (a) and a^* - (b) axes. For clarity, the vertical axis of the data $T \leq 15$ K is shifted. The data obtained in the field-up and field-down procedure is shown by filled and open symbols, respectively.

Material Fig. S6 [37]) where the phonon thermal conduction is enhanced by suppressing a magnon–phonon scattering by opening a magnon gap (see Supplemental Material Sec. IV [37]). This enhancement of κ_{xx} at 15 T (Fig. 1) shows the presence of a strong spin–phonon coupling suppressing κ_{xx} at 0 T in this compound. The residual of κ_{xx}/T in the zero-temperature limit is vanishingly small for the whole field range we measured (see Supplemental Material Fig. S7 [37]), showing the absence of itinerant gapless excitations.

Figure 2 shows the field dependence of κ_{xx} at fixed temperatures. The field dependence of κ_{xx} is negligible above T_N except for the small increase at the highest field. This increase of κ_{xx} could be attributed to an increase of the phonon conduction caused by a field suppression effect on the spin fluctuation. Below T_N , κ_{xx} starts to depend on the magnetic field, with features at critical fields of the AFM phases determined by previous studies [25,30,33] (B_{c1} and B_{c2} for $B \parallel a$, and B_{c1}^* , B_{c2}^* , and B_{c3}^* for $B \parallel a^*$), as marked by arrows in Fig. 2. In $B \parallel a$, the field dependence of dM/dB shows a shoulder at $B_{c1} \sim 7.6$ T and a peak at $B_{c2} \sim 9.8$ T [33]. Corresponding to these critical fields, κ_{xx} shows the peak at B_{c1} and the dip at B_{c2} , as shown in Fig. 2(a). On the other hand, in $B \parallel a^*$, three critical fields (denoted as B_{c1}^* , B_{c2}^* , and B_{c3}^*) are found in the field dependence of dM/dB [33]. As shown in Fig. 2(b), κ_{xx} shows a sharp jump at $B_{c1}^* \sim 6$ T with a large magnetic hysteresis, demonstrating the first-order transition at B_{c1}^* . This first-order transition is also observed as the jump in the magnetization of our sample in $B \parallel a^*$ (see Supplemental Material Fig. S3(b) [37]) [25,30,33]. In contrast to κ_{xx} in $B \parallel a$, only small humps are observed at B_{c2}^* and B_{c3}^* in $B \parallel a^*$. As κ_{xx} of a magnetic insulator is given by the sum of the phonon contribution κ_{xx}^{ph} and the magnon contribution κ_{xx}^{mag} , the field dependence of κ_{xx} of this compound can be understood in terms of the field effect of the magnon gap on κ_{xx}^{ph} and κ_{xx}^{mag} (see Supplemental Material Sec. VI [37]).

Our main finding is the finite planar κ_{xy} in the AFM phase for both $B \parallel a$ [κ_{xy}^a , Fig. 3(a)] and $B \parallel a^*$ [$\kappa_{xy}^{a^*}$, Fig. 3(b)]. We averaged the data of κ_{xy}^a/T obtained in the field-up and

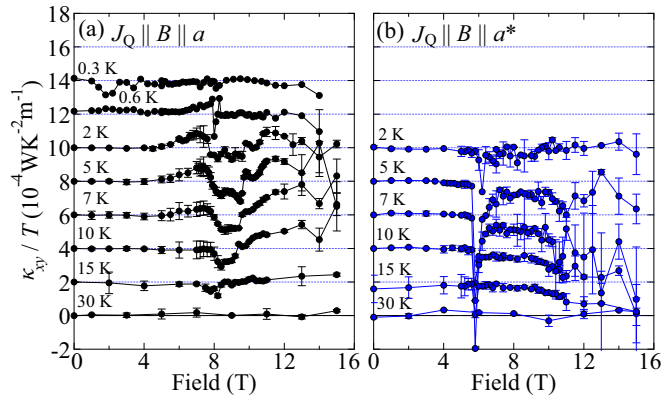


FIG. 3. The field dependence of the thermal Hall conductivity divided by the temperature for $B \parallel a$ (a) and $B \parallel a^*$ (b) at different temperatures. The data are shifted by a constant amount for clarity. The error bars show the deviation of the data in the field-up and field-down measurements.

field-down procedures except for that measured in the DR ($T < 2$ K). On the other hand, we present only the field-up data of $\kappa_{xy}^{a^*}/T$ to avoid mixing the hysteretic field dependence at B_{c1}^* (see Supplemental Material Fig. S8 [37] for all the data in each measurement). As shown in Fig. 3, whereas κ_{xy}/T is virtually absent above T_N , a finite κ_{xy}/T is observed in the AFM phase below T_N in both field directions. In $B \parallel a$, κ_{xy}^a/T gradually increases up to B_{c1} , which is followed by a sign change to negative κ_{xy}^a at B_{c1} , and another sign change to positive κ_{xy}^a at B_{c2} . In $B \parallel a^*$, $\kappa_{xy}^{a^*}$ shows a sharp negative peak at the first-order transition at B_{c1}^* , which is followed by a constant negative $\kappa_{xy}^{a^*}$ up to the highest fields. We note that the sharp negative anomaly of $\kappa_{xy}^{a^*}$ at B_{c1}^* at 2 K is more pronounced in the field-down measurements (see Supplemental Material Fig. S8 [37]). We also note that the planar THE observed in $\text{Na}_2\text{Co}_2\text{TeO}_6$ is completely different from “planar Hall effects” studied in ferromagnets [38] and Weyl semimetals [39], which are *symmetric* with respect to the field direction. In sharp contrast, the planar THE observed in this compound only comes from the *asymmetric* component in the transverse temperature difference (see Supplemental Material Sec. I [37]).

To investigate the origin of the planar THE, we turn to the temperature dependence of κ_{xy}/T at the selected fields (see arrows in Fig. 5). As shown in Fig. 4, the temperature dependence of κ_{xy}/T shows a peak at 4 to 10 K, which is followed by a decrease of $|\kappa_{xy}/T|$ to zero as $T \rightarrow 0$ K for both field directions. Remarkably, we find that, although κ_{xx}/T at 10 T features one phonon peak at approximately 30 K, κ_{xx}/T at 7, 9, and 11 T shows the second lower-temperature peak at approximately 5 K, which almost coincides with the peak of κ_{xy}/T at 7 and 11 T.

Let us first focus on the origin of the planar THE observed in $\text{Na}_2\text{Co}_2\text{TeO}_6$, which could be caused by Majorana fermions [5], phonons [40], or topological magnons [12–15]. The magnitude of κ_{xy}/T of the Majorana fermions in the Kitaev QSL is expected to show the half-quantized value $\kappa_{xy}^{2D}/T = (\pi/12)(k_B^2/\hbar)$, where k_B is the Boltzmann constant and \hbar is the reduced Planck constant. This half-quantized

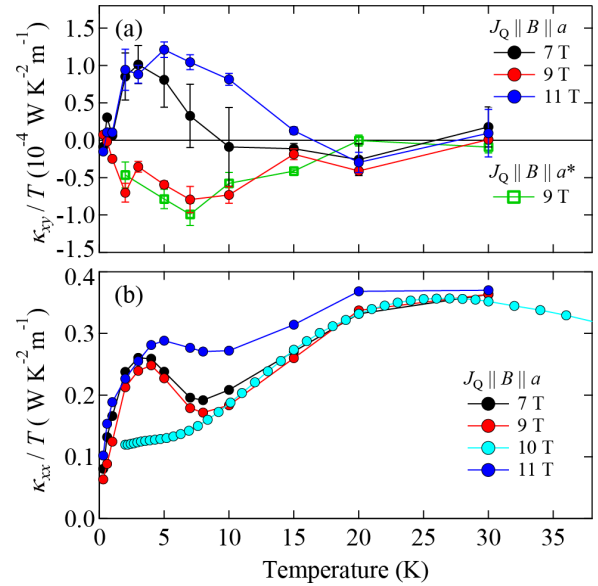


FIG. 4. The temperature dependence of κ_{xy}/T (a) and κ_{xx}/T (b) at 7, 9, and 11 T for $B \parallel a$, and at 9 T for $B \parallel a^*$. The temperature dependence of κ_{xx}/T at 10 T, the same data shown in Fig. 1(a), is also shown for comparison.

thermal Hall conductance per one layer corresponds to $\kappa_{xy}/T = (\kappa_{xy}^{2D}/d)/T \sim 8.47 \times 10^{-4} \text{ W K}^{-2} \text{ m}^{-1}$ in this compound, where $d = 0.559 \text{ nm}$ is the interlayer distance [26]. However, as shown in Figs. 3 and 4, κ_{xy}/T observed in $\text{Na}_2\text{Co}_2\text{TeO}_6$ remains about one order of magnitude smaller than the half-quantized value. In addition, although κ_{xy}/T of fermions should stay constant in the zero-temperature limit, κ_{xy}/T of $\text{Na}_2\text{Co}_2\text{TeO}_6$ approaches zero with lowering temperature (Fig. 4), showing the bosonic nature of the elementary excitations. In $\alpha\text{-RuCl}_3$, it is pointed out that the half-quantized κ_{xy}/T is suppressed in the low-quality samples with suppressed κ_{xx}^{ph} [8,9]. This is clearly not the case for our sample, in which the phonon with a long mean free path (see Supplemental Material Fig. S6 [37]) is observed. Indeed, the magnitude of κ_{xx} of our sample at 15 T [Figs. 1(a) and 1(b)] and that of the sample showing the half-quantized κ_{xy} in $\alpha\text{-RuCl}_3$ below the Néel temperature [8], in which κ_{xx}^{ph} without the strong magnon–phonon scattering specific to each materials can be observed, are similar in these two materials (approximately $6 \text{ W K}^{-1} \text{ m}^{-1}$ at 5 K, for example). It is also pointed out that a good thermalization between the Majorana fermions and phonons is necessary to observe the half-quantized κ_{xy}/T in the Kitaev QSL [41,42]. Although an accurate estimation for the Majorana–phonon coupling in $\text{Na}_2\text{Co}_2\text{TeO}_6$ is not possible at this moment, this coupling should be related to the spin–phonon coupling that gives rise to the positive magnetothermal conductivity. As shown in Fig. 2, the thermal conductivity at 5 K increases by a factor of eight under the in-plane field of 15 T, which is much larger than that in $\alpha\text{-RuCl}_3$ at a similar temperature and field [43]. Therefore, it is implausible that the suppressed κ_{xy}/T is caused by a much smaller coupling between the Majorana fermions and phonons in $\text{Na}_2\text{Co}_2\text{TeO}_6$ than that in $\alpha\text{-RuCl}_3$. Furthermore, a finite κ_{xy} is prohibited in $B \parallel a^*$ by

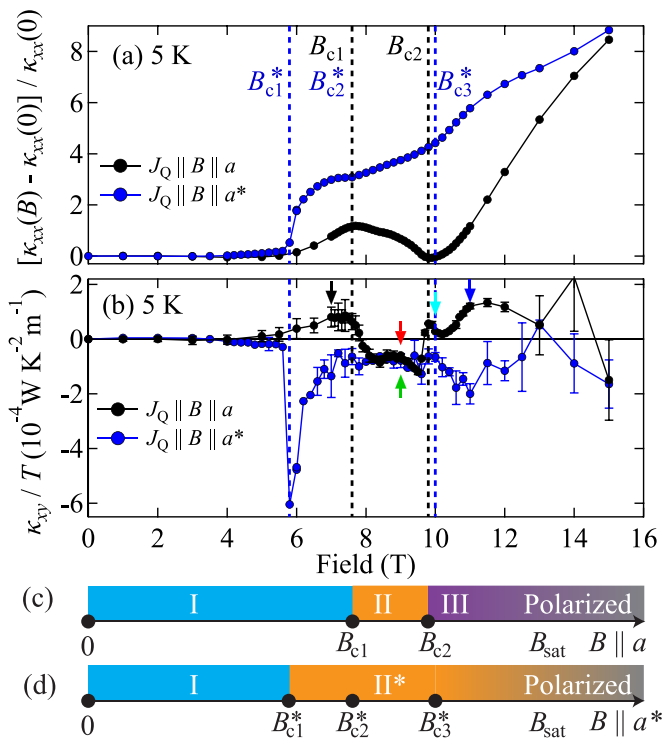


FIG. 5. (a, b) A comparison of the field dependence of the longitudinal thermal conductivity (κ_{xx}) (a) and the planar thermal Hall conductivity (κ_{xy}) (b) for $B \parallel a$ (black) and $B \parallel a^*$ (blue) at 5 K. The critical fields are also marked by dashed lines. The arrows indicate the field used in the data of the same color in Fig. 4. (c, d) The suggested magnetic phases of $\text{Na}_2\text{Co}_2\text{TeO}_6$ in $B \parallel a$ (c) and $B \parallel a^*$ (d), drawn from our thermal transport measurements.

the two-fold rotation symmetry around the a^* -axis in a Kitaev-Heisenberg paramagnet [13–15], demonstrating the presence of a long-range ordered state that breaks the two-fold rotation symmetry in $B \parallel a^*$. Therefore, we conclude that the emergence of Majorana fermions is unlikely in $\text{Na}_2\text{Co}_2\text{TeO}_6$.

As shown in Fig. 4, the planar THE develops below T_N , suggesting a dominant contribution from topological magnons in $\text{Na}_2\text{Co}_2\text{TeO}_6$. The abrupt sign changes of κ_{xy} observed at the magnetic phase boundaries in the AFM phase [Fig. 5(b)] also suggest that the planar THE arises from the intrinsic Berry phase effect of the topological magnons, because the sign changes can be most naturally attributed to a redistribution of the Berry curvature of the magnons by the magnetic transitions. In fact, the numerical calculations demonstrate sign changes of κ_{xy} of the magnons at the magnetic phase transitions in the Kitaev–Heisenberg model [13,15,44]. On the other hand, it would be unlikely that the abrupt sign changes are caused by a reversal of scattering direction upon collisions of magnons with extrinsic impurities at the magnetic transitions.

Remarkably, a recent report of κ_{xy} done in $B \parallel c$ [35] shows a very different temperature dependence from our planar THE. In $B \parallel c$, a large κ_{xy} emerges far above T_N , with a similar temperature dependence with that of κ_{xx} . This good scaling between κ_{xy} and κ_{xx} is regarded as the key feature of the phonon THEs [45,46], suggesting a dominant phonon contribution in κ_{xy} under $B \parallel c$, which could be caused by

the strong spin–phonon coupling suppressing κ_{xx} . In sharp contrast, the peak temperature of our planar κ_{xy}/T (4 to 10 K) is far below the phonon peak of κ_{xx}/T at about 30 K above T_N (Fig. 4), supporting that the dominant contribution of the planar THE comes from the topological magnons rather than phonons acting in $B \parallel c$.

We thus conclude that the planar THE observed in $\text{Na}_2\text{Co}_2\text{TeO}_6$ mainly stems from the topological magnons in long-range ordered phases [12–15], whereas, given the current insufficient knowledge about the details of the magnetic order and the spin Hamiltonian of this compound, it remains as future work to identify the magnon bands that can reproduce the κ_{xy} data. It should be noted that phonons may play a certain role in assisting the planar THE through spin–phonon coupling [47–51]. As shown in Fig. 4(b), the peak temperature of κ_{xy}/T at 7 and 11 T coincides with the second peak of κ_{xx}/T caused by the field-enhancing effect on κ_{xx}^{ph} (see Supplemental Material Sec. VI [37]). This coincidence may suggest that κ_{xy} is enhanced through a spin–phonon coupling to the magnetic moment that develops below T_N , as suggested in a kagome antiferromagnet [50] and a van der Waals magnet [51].

Next, we discuss the field evolution of the phase transitions in the AFM phase of $\text{Na}_2\text{Co}_2\text{TeO}_6$, inferred from the field dependence of κ_{xx} and κ_{xy} at 5 K (Fig. 5). In $B \parallel a$, the gradual field-induced increase of κ_{xx} and κ_{xy}^a/T suggests that the zero-field phase [denoted as phase I shown in Fig. 5(c) and 5(d)] seems to persist up to B_{c1} . The first sign flip of κ_{xy}^a at B_{c1} and the peak in the field dependence of κ_{xx} show a magnetic phase transition at B_{c1} into a different magnetic phase (phase II), with a dominant negative Berry phase distribution and a field-induced suppression on κ_{xx} . The next sign flip of κ_{xy}^a at B_{c2} along with the marked change in the field dependence of κ_{xx} indicates the existence of another magnetic phase (phase III) above B_{c2} . We note that the good correspondence between the field dependence of κ_{xx} and κ_{xy}^a/T is observed not only at 5 K, but also at higher temperatures (see Supplemental Material Fig. S9 [37]). These sign changes of the Berry phase distributions between the different magnetic states, suggested by our planar THE measurements, provide essential information for future studies to identify the magnetic states by calculating κ_{xy} of them.

In $B \parallel a^*$, the sharp jumps both in κ_{xx} and $\kappa_{xy}^{a^*}/T$ indicate the first-order phase transition into phase II* at B_{c1}^* under $B \parallel a^*$. The sharp jump in κ_{xx} is more pronounced at lower temperatures [Fig. 2(b)], whereas the magnitude of $\kappa_{xy}^{a^*}/T$ shows a peak at around 7 K [Fig. 4(a)]. This different thermal behavior is caused by the disparate transport processes between κ_{xx} and κ_{xy} . The former is dictated by the suppression of the magnon–phonon scattering by opening a magnon gap, which is more pronounced at lower temperatures. On the other hand, the latter reflects the boson occupation in the energy bands with a finite Berry curvature, showing a peak when the thermal energy coincides with the energy bands with the largest Berry curvature [19]. In contrast to the case in $B \parallel a$, both the field dependences of κ_{xx} and $\kappa_{xy}^{a^*}$ in $B \parallel a^*$ are essentially featureless above B_{c1}^* , except for small bumps in κ_{xx} . Given the clear anomalies in dM/dB at B_{c2}^* and B_{c3}^* [33], the featureless field dependence of $\kappa_{xy}^{a^*}/T$ is rather an

unexpected result. These results suggest that phase II* continuously changes to the spin-polarized phase, which should be scrutinized by future NMR or neutron scattering measurements. The negative $\kappa_{xy}^{a^*}$ in phase II* shows the emergence of topological magnon bands with a negative Chern number in phase II*. Remarkably, both the magnitude and the field dependence of $\kappa_{xy}^{a^*}/T$ are very similar to those of κ_{xy}^a/T for 8 to 10 T in phase II, whereas the field effect on κ_{xx} is opposite in these two phases. This similarity in κ_{xy} with anisotropic field dependence in κ_{xx} may suggest that phases II and II* share a similar Chern number distribution despite the different magnetic structures between them. Such different magnetic structures in different field directions in the two-dimensional honeycomb plane are shown by the numerical calculations [14,44], and are indeed observed in α -RuCl₃ by the neutron scattering experiments under $B \parallel [110]$ and $B \parallel [100]$ [52].

Finally, we discuss the magnetic state above B_{c3} and B_{c3}^* . Although previous studies [30,33] have suggested the emergence of a disordered state above B_{c3} or B_{c3}^* , the finite $\kappa_{xy}^{a^*}/T$ above B_{c1}^* reveals the presence of a magnetic order that breaks the two-fold rotation symmetry around the a^* -axis in $B \parallel a^*$. Given the continuous field dependence of $\kappa_{xy}^{a^*}/T$ and κ_{xx} for $B \parallel a^*$, this ordered phase persists above B_{c1}^* up to B_{sat} . On the other hand, the sign reversal of κ_{xy}^a at B_{c3} shows an appearance of a different magnetic state for $B_{c3} < B < B_{\text{sat}}$ for $B \parallel a$. The positive κ_{xy}^a and the vanishing κ_{xy}^a/T in the zero-temperature limit at 11 T [Fig. 4(a)] are consistent with another magnetically ordered state that possesses topological magnons with a positive Chern number. However, the absence of a clear

thermodynamical phase transition above B_{c3} may suggest that phase III is a disordered state including a partially polarized state [33], requiring further microscopic measurements to reveal the details of phase III.

In summary, from our planar thermal Hall measurements in Na₂Co₂TeO₆, we find a finite planar κ_{xy} with sign changes at critical magnetic fields applied along the a - and a^* -axes, suggesting a THE of topological magnons. The finite planar κ_{xy} in $B \parallel a^*$ reveals that a magnetically ordered state breaking the two-fold rotation symmetry around the a^* -axis appears above B_{c1}^* , which persists up to B_{sat} . We further find three different magnetic phases in $B \parallel a$ that can be characterized by the different Chern numbers of the topological magnons. Our findings, especially for the sign changes of the planar κ_{xy} , put strong constraints on identifying the magnetic state in this compound.

This work was supported by Grants-in-Aid for Scientific Research (KAKENHI) (Grants No. JP19H01848 and No. JP19K21842) and the Murata Science Foundation. M.A. was supported by JST SPRING (Grant No. JPMJSP2108). R.S. acknowledges the financial support provided by the Ministry of Science and Technology in Taiwan (Project No. MOST-110-2112-M-001-065-MY3) and the Academia Sinica budget (AS-iMATE-111-12). The work at Sungkyunkwan University is supported by the National Research Foundation (NRF) of Korea (Grants No. 2020R1A2C3012367 and No. 2020R1A5A1016518). We thank J. Nasu for fruitful discussions.

-
- [1] F. D. M. Haldane, Model for a Quantum Hall Effect without Landau Levels: Condensed-Matter Realization of the Parity Anomaly, *Phys. Rev. Lett.* **61**, 2015 (1988).
 - [2] C.-Z. Chang *et al.*, Experimental observation of the quantum anomalous Hall effect in a magnetic topological insulator, *Science* **340**, 167 (2013).
 - [3] H. Katsura, N. Nagaosa, and P. A. Lee, Theory of the Thermal Hall Effect in Quantum Magnets, *Phys. Rev. Lett.* **104**, 066403 (2010).
 - [4] R. Matsumoto, R. Shindou, and S. Murakami, Thermal Hall effect of magnons in magnets with dipolar interaction, *Phys. Rev. B* **89**, 054420 (2014).
 - [5] A. Kitaev, Anyons in an exactly solved model and beyond, *Ann. Phys.* **321**, 2 (2006).
 - [6] G. Jackeli and G. Khaliullin, Mott Insulators in the Strong Spin-Orbit Coupling Limit: From Heisenberg to a Quantum Compass and Kitaev Models, *Phys. Rev. Lett.* **102**, 017205 (2009).
 - [7] Y. Kasahara *et al.*, Majorana quantization and half-integer thermal quantum Hall effect in a Kitaev spin liquid, *Nature (London)* **559**, 227 (2018).
 - [8] M. Yamashita, J. Gouchi, Y. Uwatoko, N. Kurita, and H. Tanaka, Sample dependence of half-integer quantized thermal Hall effect in the Kitaev spin-liquid candidate α -RuCl₃, *Phys. Rev. B* **102**, 220404(R) (2020).
 - [9] T. Yokoi *et al.*, Half-integer quantized anomalous thermal Hall effect in the Kitaev material candidate α -RuCl₃, *Science* **373**, 568 (2021).
 - [10] J. A. N. Bruin, R. R. Claus, Y. Matsumoto, N. Kurita, H. Tanaka, and H. Takagi, Robustness of the thermal Hall effect close to half-quantization in α -RuCl₃, *Nat. Phys.* **18**, 401 (2022).
 - [11] Y.-F. Yang, G.-M. Zhang, and F.-C. Zhang, Universal Behavior of the Thermal Hall Conductivity, *Phys. Rev. Lett.* **124**, 186602 (2020).
 - [12] L. Zhang, J. Ren, J.-S. Wang, and B. Li, Topological magnon insulator in insulating ferromagnet, *Phys. Rev. B* **87**, 144101 (2013).
 - [13] L. E. Chern, E. Z. Zhang, and Y. B. Kim, Sign Structure of Thermal Hall Conductivity and Topological Magnons for In-Plane Field Polarized Kitaev Magnets, *Phys. Rev. Lett.* **126**, 147201 (2021).
 - [14] E. Z. Zhang, L. E. Chern, and Y. B. Kim, Topological magnons for thermal Hall transport in frustrated magnets with bond-dependent interactions, *Phys. Rev. B* **103**, 174402 (2021).
 - [15] S. Koyama and J. Nasu, Field-angle dependence of thermal Hall conductivity in a magnetically ordered Kitaev-Heisenberg system, *Phys. Rev. B* **104**, 075121 (2021).
 - [16] J. Romhányi, K. Penc, and R. Ganesh, Hall effect of triplons in a dimerized quantum magnet, *Nat. Commun.* **6**, 6805 (2015).
 - [17] K. A. van Hoogdalem, Y. Tserkovnyak, and D. Loss, Magnetic texture-induced thermal Hall effects, *Phys. Rev. B* **87**, 024402 (2013).
 - [18] L. Kong and J. Zang, Dynamics of an Insulating Skyrmion Under a Temperature Gradient, *Phys. Rev. Lett.* **111**, 067203 (2013).

- [19] M. Akazawa, H.-Y. Lee, H. Takeda, Y. Fujima, Y. Tokunaga, T. Arima, J. H. Han, and M. Yamashita, Topological thermal Hall effect of magnons in magnetic skyrmion lattice, *Phys. Rev. Res.* **4**, 043085 (2022).
- [20] H. Liu and G. Khaliullin, Pseudospin exchange interactions in d^7 cobalt compounds: Possible realization of the Kitaev model, *Phys. Rev. B* **97**, 014407 (2018).
- [21] R. Sano, Y. Kato, and Y. Motome, Kitaev-Heisenberg Hamiltonian for high-spin d^7 Mott insulators, *Phys. Rev. B* **97**, 014408 (2018).
- [22] H. Liu, J. Chaloupka, and G. Khaliullin, Kitaev Spin Liquid in $3d$ Transition Metal Compounds, *Phys. Rev. Lett.* **125**, 047201 (2020).
- [23] L. Viciu, Q. Huang, E. Morosan, H. W. Zandbergen, N. I. Greenbaum, T. McQueen, and R. J. Cava, Structure and basic magnetic properties of the honeycomb lattice compounds $\text{Na}_2\text{Co}_2\text{TeO}_6$ and $\text{Na}_3\text{Co}_2\text{SbO}_6$, *J. Solid State Chem.* **180**, 1060 (2007).
- [24] M. Songvilay *et al.*, Kitaev interactions in the Co honeycomb antiferromagnets $\text{Na}_3\text{Co}_2\text{SbO}$ and $\text{Na}_2\text{Co}_2\text{TeO}_6$, *Phys. Rev. B* **102**, 224429 (2020).
- [25] G. Lin *et al.*, Field-induced quantum spin disordered state in spin-1/2 honeycomb magnet $\text{Na}_2\text{Co}_2\text{TeO}_6$, *Nat. Commun* **12**, 5559 (2021).
- [26] A. M. Samarakoon, Q. Chen, H. Zhou, and V. O. Garlea, Static and dynamic magnetic properties of honeycomb lattice antiferromagnets $\text{Na}_2\text{M}_2\text{TeO}_6$, $M = \text{Co}$ and Ni , *Phys. Rev. B* **104**, 184415 (2021).
- [27] C. Kim *et al.*, Antiferromagnetic Kitaev interaction in $J_{\text{eff}} = 1/2$ cobalt honeycomb materials $\text{Na}_3\text{Co}_2\text{SbO}_6$ and $\text{Na}_2\text{Co}_2\text{TeO}_6$, *J. Phys. Condens. Matter* **34**, 045802 (2021).
- [28] E. Lefrançois *et al.*, Magnetic properties of the honeycomb oxide $\text{Na}_2\text{Co}_2\text{TeO}_6$, *Phys. Rev. B* **94**, 214416 (2016).
- [29] A. K. Bera, S. M. Yusuf, A. Kumar, and C. Ritter, Zigzag antiferromagnetic ground state with anisotropic correlation lengths in the quasi-two-dimensional honeycomb lattice compound $\text{Na}_2\text{Co}_2\text{TeO}_6$, *Phys. Rev. B* **95**, 094424 (2017).
- [30] W. Yao and Y. Li, Ferrimagnetism and anisotropic phase tunability by magnetic fields in $\text{Na}_2\text{Co}_2\text{TeO}_6$, *Phys. Rev. B* **101**, 085120 (2020).
- [31] W. Chen *et al.*, Spin-orbit phase behavior of $\text{Na}_2\text{Co}_2\text{TeO}_6$ at low temperatures, *Phys. Rev. B* **103**, L180404 (2021).
- [32] C. H. Lee, S. Lee, Y. S. Choi, Z. H. Jang, R. Kalaivanan, R. Sankar, and K.-Y. Choi, Multistage development of anisotropic magnetic correlations in the Co-based honeycomb lattice $\text{Na}_2\text{Co}_2\text{TeO}_6$, *Phys. Rev. B* **103**, 214447 (2021).
- [33] X. Hong *et al.*, Strongly scattered phonon heat transport of the candidate Kitaev material $\text{Na}_2\text{Co}_2\text{TeO}_6$, *Phys. Rev. B* **104**, 144426 (2021).
- [34] N. Li *et al.*, Sign switchable magnon thermal Hall conductivity in an antiferromagnet, *arXiv:2201.11396* (2022).
- [35] H. Yang *et al.*, Significant thermal Hall effect in the $3d$ cobalt Kitaev system $\text{Na}_2\text{Co}_2\text{TeO}_6$, *Phys. Rev. B* **106**, L081116 (2022).
- [36] M. Yamashita *et al.*, Thermal-transport studies of kagomé antiferromagnets, *J. Phys. Condens. Matter* **32**, 74001 (2019).
- [37] See Supplemental Material at <http://link.aps.org/supplemental/10.1103/PhysRevResearch.4.L042035> for (1) the details of the thermal-transport measurements, (2) extended data of the magnetization and the thermal conductivity, (3) the sample dependence of the thermal Hall effect, (4) estimation of the phonon mean free path, (5) the residual of κ_{xx}/T in the zero-temperature limit, (6) field effect on the phonon contribution and the magnon contribution in κ_{xx} , (7) the field dependence of κ_{xy}/T in the field-up and the field-down measurements, and (8) the field dependence of κ_{xx} and κ_{xy}/T at high temperatures.
- [38] V. D. Ky, Planar Hall and Nernst effect in ferromagnetic metals, *Phys. Status Solidi B* **22**, 729 (1967).
- [39] S. Nandy, G. Sharma, A. Taraphder, and S. Tewari, Chiral Anomaly as the Origin of the Planar Hall Effect in Weyl Semimetals, *Phys. Rev. Lett.* **119**, 176804 (2017).
- [40] L. Zhang, J. Ren, J.-S. Wang, and B. Li, Topological Nature of the Phonon Hall Effect, *Phys. Rev. Lett.* **105**, 225901 (2010).
- [41] Y. Vinkler-Aviv and A. Rosch, Approximately Quantized Thermal Hall Effect of Chiral Liquids Coupled to Phonons, *Phys. Rev. X* **8**, 031032 (2018).
- [42] M. Ye, G. B. Halász, L. Savary, and L. Balents, Quantization of the Thermal Hall Conductivity at Small Hall Angles, *Phys. Rev. Lett.* **121**, 147201 (2018).
- [43] R. Hentrich *et al.*, High-field thermal transport properties of the Kitaev quantum magnet $\alpha\text{-RuCl}_3$: Evidence for low-energy excitations beyond the critical field, *Phys. Rev. B* **102**, 235155 (2020).
- [44] S. Li and S. Okamoto, Thermal Hall effect in the Kitaev-Heisenberg system with spin-phonon coupling, *Phys. Rev. B* **106**, 024413 (2022).
- [45] X. Li, B. Fauqué, Z. Zhu, and K. Behnia, Phonon Thermal Hall Effect in Strontium Titanate, *Phys. Rev. Lett.* **124**, 105901 (2020).
- [46] G. Grissonnanche *et al.*, Chiral phonons in the pseudogap phase of cuprates, *Nat. Phys.* **16**, 1108 (2020).
- [47] X. Zhang, Y. Zhang, S. Okamoto, and D. Xiao, Thermal Hall Effect Induced by Magnon-Phonon Interactions, *Phys. Rev. Lett.* **123**, 167202 (2019).
- [48] R. Takahashi and N. Nagaosa, Berry Curvature in Magnon-Phonon Hybrid Systems, *Phys. Rev. Lett.* **117**, 217205 (2016).
- [49] G. Go, S. K. Kim, and K.-J. Lee, Topological Magnon-Phonon Hybrid Excitations in Two-Dimensional Ferromagnets with Tunable Chern Numbers, *Phys. Rev. Lett.* **123**, 237207 (2019).
- [50] M. Akazawa, M. Shimozawa, S. Kittaka, T. Sakakibara, R. Okuma, Z. Hiroi, H.-Y. Lee, N. Kawashima, J. H. Han, and M. Yamashita, Thermal Hall Effects of Spins and Phonons in Kagome Antiferromagnet Cd-Kapellasite, *Phys. Rev. X* **10**, 041059 (2020).
- [51] H. Zhang, C. Xu, C. Carnahan, M. Sretenovic, N. Suri, D. Xiao, and X. Ke, Anomalous Thermal Hall Effect in an Insulating Van Der Waals Magnet, *Phys. Rev. Lett.* **127**, 247202 (2021).
- [52] C. Balz, L. Janssen, P. Lampen-Kelley, A. Banerjee, Y. H. Liu, J. Q. Yan, D. G. Mandrus, M. Vojta, and S. E. Nagler, Field-induced intermediate ordered phase and anisotropic interlayer interactions in $\alpha\text{-RuCl}_3$, *Phys. Rev. B* **103**, 174417 (2021).